

# Extragalactic radio source evolution under the dual-population unification scheme

C.A.Jackson<sup>1</sup> & J.V.Wall<sup>2</sup>

<sup>1</sup>*Institute of Astronomy, University of Cambridge, Madingley Road, Cambridge, CB3 OHA, UK*

<sup>2</sup>*Royal Greenwich Observatory, Madingley Road, Cambridge, CB3 OEZ, UK*

arXiv:astro-ph/9808054v1 7 Aug 1998

Accepted 1998 ??? ?. Received 1998 ??? ??. in original form 6 Aug 1998

## ABSTRACT

We show that a dual-population unification scheme provides a successful paradigm with which to describe the evolution and beaming of all bright extragalactic radio sources. The paradigm consists of two intrinsic radio-source populations, based on the two distinct radio-galaxy morphologies of Fanaroff-Riley classes I and II. These represent the ‘unbeamed’ or ‘side-on’ parent populations of steep radio spectra; the ‘beamed’ source types including flat-spectrum quasars and BL Lac objects, arise through the random alignment of their radio-axis to our line-of-sight where Doppler-beaming of the relativistic radio jets produces highly anisotropic radio emission.

We develop the model in two stages. In the first stage the source space density as a function of cosmic epoch is determined for the two parent populations, and for this we use low-frequency source-count and identification data to avoid biases due to Doppler-enhanced radio emission. The second stage defines the beaming models for each population, using high-frequency survey data and in particular the 5-GHz source count in which at high flux densities the flat- and steep-spectrum sources contribute in similar measure. We assume that the flat-spectrum objects, quasars and BL Lac objects are ‘beamed’ versions of FRI and FRII objects in which the close alignment of radio-axis with line-of-sight has changed the radio appearance into a core-dominated (flat-spectrum) object. We adopt a simple parameterisation of the beaming, orient the parent populations at random with a Monte-Carlo process, and use a minimisation process to determine beaming parameters which yield a best fit to the 5-GHz source count. The best-fit parameters are found to be in good agreement with those measured observationally for individual radio sources. In this, the model accurately reproduces the change in source-count form with frequency. Indeed the unified-scheme paradigm has great predictive power, and we show how the model successfully describes several additional and independent data sets.

**Key words:** galaxies:evolution, galaxies:jets, quasars:general, radio continuum:galaxies

## 1 INTRODUCTION

The dramatic space density evolution of radio-loud AGNs has been shown to mirror the cosmic star formation rate (Wall 1998; Boyle & Terlevich 1998; Shaver et al. 1998). Similar strong epoch dependence is seen in the faint blue galaxy population (Metcalfe et al. 1995; Roche et al. 1996), IRAS galaxies (Saunders et al. 1990) and the radio-bright starbursting galaxies (Condon 1984; Rowan-Robinson et al. 1993). These correlated epoch-dependences provide enticing

clues towards understanding AGN physics, in the context of triggers to activity such as coalescence of critical mass, merging, fuel supply, and the lobe confinement provided by an evolving IGM.

Our concept of the radio-source populations developed slowly. The work of Longair (1966) and collaborators (Doroshkevich, Longair & Zeldovich 1970) demonstrated conclusively the dependence of the radio-AGN evolution on radio luminosity: at redshifts  $> 1$  the most powerful radio sources showed space-density enhancements by factors of  $> 10^3$  over present-day densities, whereas the less-powerful sources showed little or no enhancement. Subsequently Fanaroff & Riley (1974) demonstrated a morpho-

\* Current address Department of Astrophysics, School of Physics, University of Sydney, NSW 2006, Australia

logical dichotomy: double-lobe radio sources with regions of highest surface brightness close to the nucleus (Fanaroff-Riley type (FRI)) have radio luminosities consistently lower than those with highest surface brightness at the extremities (FRII). The FRI – FRII division occurs approximately at a radio power of  $\log_{10}(P_{151 \text{ MHz}}) \sim 10^{25} \text{ W Hz}^{-1} \text{ sr}^{-1}$ , close to the luminosity dividing strongly-evolving radio sources from those showing little evolution. On the basis of this coincidence, Wall (1980) suggested that the FRI population showed near-constant space density while the FRII objects evolved strongly with cosmic epoch.

The early surveys were at relatively low frequencies and catalogued predominantly steep-spectrum radio galaxies of extended double-lobed structures. During the late 1960s and the 1970s surveys at frequencies  $> 2 \text{ GHz}$  found a large number of radio AGN whose spectra did not decrease monotonically with frequency - sources of hard radio spectra, described (unfortunately) as ‘flat spectrum’ objects. In contrast to the host objects of steep radio spectra, predominantly giant ellipticals, the majority of the flat-spectrum objects were identified with QSOs (quasars) or BL Lac objects and had compact radio structures, unresolved until mapped with VLBI. Schmidt (1976) and Mason & Wall (1977) claimed that despite their apparent high radio luminosity of such objects, they showed little evolution. This result was disputed and eventually the comprehensive analysis of Dunlop & Peacock (1990) showed that qualitatively the flat-spectrum population showed a similar evolutionary behaviour to the steep-spectrum population: luminosity-dependent density evolution was required. However, at a particular radio luminosity, the space density evolution of the flat-spectrum population is *less* than that of the steep-spectrum population. At the time, physical connection between the steep-spectrum and flat-spectrum populations were not considered in such analyses.

It was the discovery of relativistic expansion (Cohen et al. 1971; Moffat et al. 1972) through repeated VLBI measurements of the brighter ‘flat-spectrum’ sources which laid the foundation for unification paradigms. Whilst relativistic motion is the primary mechanism giving rise to anisotropic radio emission in radio-loud AGN, a second mechanism, the presence of a dusty molecular torus (Antonucci & Miller 1985) was invoked to explain the optical emission characteristics of some sources. From these two physical mechanisms the paradigm emerged in which the random orientation of a ‘parent’ population on the plane of the sky gave rise to radio sources of apparently diverse type. The *unified schemes* proposed for radio-loud AGN (Scheuer & Readhead 1979; Orr & Browne 1982; Scheuer 1987; Barthel 1989) have both radio and optical appearance governed by proximity of the line-of-sight to the radio (presumably rotation) axis. In the radio regime, close coincidence changes the morphology from an extended steep-spectrum source to a source with a dominant flat-spectrum ‘core’ from the Doppler-boosted base of the foreground jet. The optical appearance changes from galaxy as viewed side-on to quasar or BL Lac object when orientation permits a view into the torus opening angle and optical/UV radiation from the accretion disk system dominates stellar emission.

If we are to understand the physical significance of the evolution which originally suggested different populations, it is essential to delineate the populations on a physical basis.

We cannot map the evolution meaningfully until we know the physically-distinct populations for which we wish to derive it.

The primary purpose of this paper is to advance this chicken-and-egg situation in the following way. Firstly we consider the dual-population unified scheme, based on the premise that the two parent populations are FRI and FRII radio galaxies, which give rise to BL Lac objects and quasars as beamed progeny. Our basic assumption is that *all* radio sources detected above  $S_{5 \text{ GHz}} \sim 3 \text{ mJy}$  are encompassed by this scheme. Using the best available data in terms of source counts and identifications at low frequencies, we estimate the space densities of the parent populations. We then set up the unified models to define critical angles within which the line-of-sight turns these lobe-dominated sources into core-dominated sources. Using a Monte Carlo orienting process we allow free rein to the fitting process to reproduce a high-frequency radio source count. This process results in a model for the Doppler beaming of the radio jets with physical parameters which closely mirror those observed in VLBI monitoring surveys. The dual-population unified scheme makes numerous quantitative predictions which can be tested, and a number are described in this paper. Crucial further observations are delineated.

This is not the first attempt to incorporate a unification paradigm within space density analyses. Before the discovery of dusty tori, Scheuer & Readhead (1979) proposed a model of superluminal expansion for quasars with a view to explaining the ratio of radio-quiet QSOs to radio-loud quasars. A second seminal study by Orr & Browne (1982) proposed that the core-dominated quasars were aligned versions of steep-spectrum quasars based on the twin relativistic-jet model of Blandford & Rees (1974). Using the observed redshift distribution of 3C quasars and a simple beaming model they calculated the Lorentz factor,  $\gamma$ , from the observed core-to-lobe flux ratio distribution,  $R$ , for a sample of quasars. They found that the flat-spectrum quasar fractions at 2.7 GHz and 5 GHz could be reproduced by single values of  $R_T$  and  $\gamma$ . These views of unification were limited, primarily in that the dusty torus did not form part of the modelling. More recently, Urry and Padovani (1995 and references therein) considered a simple two-population unified scheme, where FRII radio galaxies are the parent population of *all* quasars and FRIs are the parent population of *all* BL Lac-type objects. They fitted the observed luminosity function for the steep-spectrum, ‘misaligned’ objects to the flat-spectrum, ‘aligned’ luminosity function, using a pure luminosity evolution model coupled with simple model of the Doppler beaming which required a large range of Lorentz factors.

In contrast, this paper starts with a definition of the two parent populations based on low-frequency data alone, and derives independent space-density descriptions for each. Using high-frequency data it then derives beaming models for each population. An embryonic version of the present model was described by Wall & Jackson (1997); the present paper adopts the same thesis and procedure, presents the data in detail, describes a refined version of evolution for the parent population and develops beaming models which provides a *distribution* of apparent jet velocities as well as core-to-lobe flux ratios. In addition, cosmological tests of the paradigm are presented.

Throughout this paper we use  $h=0.5$  and  $\Omega_0=1.0$ .

## 2 THE DUAL-POPULATION UNIFIED SCHEME

The current unification paradigm for radio-loud AGN is based on two ‘parent’ populations, namely (i) the high-radio-power FRII galaxies and (ii) the moderate-radio-power FRI galaxies. Both populations exhibit anisotropic radiation arising from superluminal motion (Doppler beaming) of the radio jets. In addition, obscuration by a dusty torus contributes to the orientation-dependent appearance of the high-power FRIIs; when the torus/rotation axis and the line-of-sight are approximately aligned, radiation from the accretion disk about the black hole dominates the galaxy emission. The orientation angle of the radio axis on the plane of the sky determines the observed characteristics and the hence the classification of the object.

In the case of the FRII radio galaxy, a side-on view reveals a lobe-dominated steep-spectrum radio source hosted by a giant elliptical galaxy, possibly with narrow emission lines of high excitation. As the observer’s line of sight comes closer to the radio axis, the object appears as a ‘steep-spectrum quasar’, the line-of-sight bringing the blue light / broad-line region of the nuclear accretion disk into view to dominate the light of the host galaxy. At close coincidence, the radio radiation becomes dominated by the Doppler-enhanced core or base of the forward jet; features may show superluminal velocities. In the case of the FRI radio galaxies, the side-on view shows a galaxy of weak-to-no narrow emission lines while the on-axis view reveals a BL Lac object of essentially featureless optical continuum and compact radio structure showing superluminal velocities.

The steep-spectrum side-on objects, FRI and FRII radio galaxies plus steep-spectrum quasars, dominate the results from low-frequency surveys, the complete samples and source counts. High-frequency radio surveys favour the radio sources of harder spectrum, *i.e.* beamed, core-dominated sources, BL Lac objects and core-dominated quasars. Raising survey frequency selects samples and source-counts dominated by objects with their radio axes close to our line-of-sight.

The hypothesis that lobe-dominated steep-spectrum and core-dominated flat-spectrum quasars are increasingly aligned versions of FRII radio galaxies is that originally proposed by Scheuer (1987); Peacock (1987); Barthel (1989). The corresponding scheme for FRI - BL Lac unification was put forward by Browne (1983); Perez-Fournon & Biermann (1984). However, there is accumulated evidence that the unified scheme is not quite so straightforward. In particular the FRII sources are *not* a homogeneous population in terms of their optical/UV spectral characteristics: Hine & Longair (1979) showed that FRIIs can have strong narrow optical/UV emission lines (class ‘A’) or only weak, if any, lines, similar to FRI sources (class ‘B’). Laing et al. (1994) showed that in the 3CRR sample of Laing, Riley & Longair (1983), this dichotomy was reflected by a clean division between high-excitation / strong-emission line objects and low-excitation / weak-to-no-emission-line objects. This dichotomy in the FRII population is reflected in the ‘dual population’ unified scheme which we propose. We suggest that

only the class ‘A’ FRII sources appear as lobe-dominated broad-line quasars, or core-dominated broad-line quasars at small angles of their radio axes to our line of sight.

The role of the low-excitation FRIIs has not been considered in unified models or space-density analyses to date. However the shape of the radio luminosity function for the FRII population shows that there must be many more low-excitation sources than high-excitation ones, given that excitation status correlates with radio power (Laing et al. 1994; Barthel 1994). If these objects have relativistically-beamed radio jets then they must show a beamed sub-population. There is strong evidence, both direct and circumstantial, that this sub-population is seen as BL Lac objects. Firstly, around some BL Lacs there are extended structures consistent in scale and power with the lobes of FRII sources (Browne et al. 1982; Kollgaard et al. 1992; Murphy, Browne & Perley 1993; Dallacasa et al. 1997). Secondly, there are too few FRIs for them to be the only class of host galaxy for BL Lacs (Owen, Ledlow & Keel 1996). Thirdly the lack of observed narrow emission lines in the parent sources, in the class-B FRII galaxies, correlates with the optical spectral properties of BL Lacs; the majority of radio galaxies of intrinsic radio luminosities more powerful than the FRI/FRII divide, show passive elliptical-galaxy spectra (Rixon, Wall & Benn 1991).

Thus our dual-population unified scheme, illustrated in Figure 1, consists of two parent populations: (a) the high-radio-power FRII radio galaxies which are the parents of *all* radio quasars and *some* BL Lac-type objects, and (b) the moderate-radio-power FRI radio galaxies which are the parents of BL Lac-type objects.

Whilst the identified classes of extragalactic radio sources are diverse (see *e.g.* Wall 1994 for a detailed discussion), we adopt the working hypothesis that all radio source types found in surveys between 0.15 and 10 GHz down to  $S_{1.4\text{ GHz}} \sim 1$  mJy belong to one of the two parent populations or to one other population, the starburst galaxies (Condon 1984; Windhorst et al. 1985). Table 1 describes types of extragalactic radio source commonly discussed in the literature; the only notable exclusion is cluster relic sources (Giovanini et al. 1993) which are so few in number and so low in space density as to have minimal impact on our analysis.

**The FRI and FRII sources** are the powerful radio sources explicitly described by the dual-population unified scheme of the previous section.

**The starburst galaxies** are late-type, in contrast to the other populations in the table. They have intrinsically-weak radio emission, and dominate radio samples at low flux densities (Windhorst et al. 1985). There is no evidence of any Doppler beaming of their radio emission; they lie outside the dual-population unified scheme. The contribution of this population is included in our analysis using previously-determined luminosity functions and evolution.

**The GPS and CSS** are ‘peaked-spectrum’ sources, objects with peaks in their radio spectra between 0.1 and 3 GHz. There is accumulating evidence that GigaHertz-Peaked Spectrum and Compact Steep-Spectrum (GPS and CSS) sources represent young stages ( $< 10^4$  yr) of FRII radio sources (Readhead 1995; Fanti, Vigotti & Di Paolo 1996). Therefore these source types are encompassed in the dual-population unified scheme given that (i) the frequency of broad-line objects in these classes is in general agreement

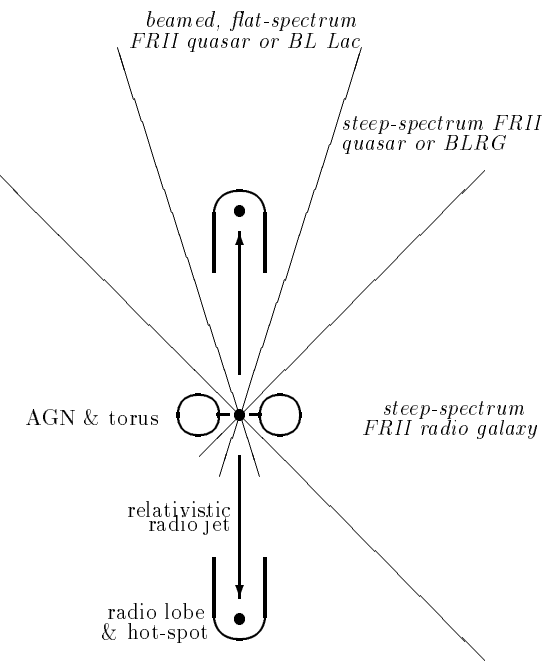


**Figure 1a.** Unified scheme for FRII radio sources.

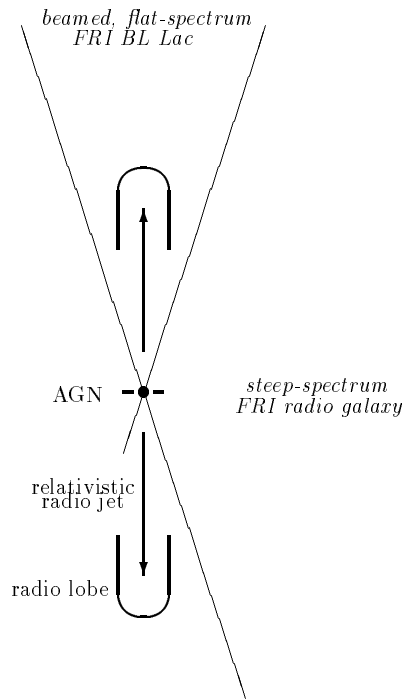


**Figure 1b.** Unified scheme for FRI radio sources.

**Table 1.** Extragalactic radio source classes.

Population	UV/optical emission-line signature	Radio spectrum $\nu \sim 5$ GHz	Class	Contribution to source count	
				$\nu \lesssim 1$ GHz	$\nu \gtrsim 1$ GHz
FRII, class A <sup>b</sup>	narrow	steep	RG	prominent	prominent
	broad	steep	RG <sup>#</sup>	prominent	prominent
	narrow	'flat'	quasar	<5%	prominent
FRII, class B <sup>b</sup>	weak/none none	steep 'flat'	RG BL Lac	prominent <5%	prominent <10%
FRI	weak/none none	steep 'flat'	RG BL Lac	prominent <5%	prominent <10%
Starburst	narrow	steep	galaxy	<1%	<1%
GPS	narrow	'flat'	RG	<1%	~5%
	broad	'flat'	quasar	<1%	~5%
CSS	narrow	steep	RG	~15%	<1%
	broad	steep	quasar	~5%	<1%

<sup>b</sup> Hine & Longair (1979) emission-line class.<sup>#</sup> alternatively a steep-spectrum quasar.

with the simple model of a broad-line region being obscured by a surrounding torus (Fanti & Fanti 1990) and (ii) superluminal motion has been observed in nearby GPS galaxies, with Lorentz factors similar to those inferred for classical FRIIs (Giovannini et al. 1995; Taylor, Vermeulen & Pearson 1995). Moreover the shortfall of peaked-spectrum quasars may due to Doppler-boosting of the forward radio jet flattening the characteristic peaked radio spectra with the result that GPS and CSS quasars are often categorized as 'normal' FRII quasars (Snellen 1997).

### 3 RADIO SOURCE SPACE DENSITIES WITHIN THE UNIFIED SCHEME

#### 3.1 Parametric models of radio source evolution

The first stage in our analysis is to determine the space density evolution of the two parent populations, allowing each to undergo quite separate evolution histories. For each of the two populations we determine its local radio luminosity function and adopt a simple parametric description of its evolution with epoch. Whilst the parametric approach has the disadvantage of applying a rigid form of evolutionary behaviour, it has the advantage of comprising only a limited set of parameters (e.g. Wall, Pearson & Longair 1980; Orr & Browne 1982; Morisawa & Takahara 1987; Rowan-Robinson et al. 1993). The alternative approach is a free-form fit (Robertson 1980; Peacock & Gull 1981; Dunlop & Peacock 1990), advantageous as there is no requirement to 'guess' the form of the evolution prior to determining an acceptable fit. However the free-form method yields a large parameter set which is difficult to manage in subsequent analyses and which does not necessarily lead to further physical understanding. A final consideration in our choice of approach is

that in describing independent evolution histories for the FRI and FRII populations, we are limited to datasets which are simply too small to use in a free-form analysis.

There are two distinct types of parameterized evolution which may be applicable to extragalactic radio sources. In the case of *luminosity evolution* (LE) the radio luminosity of sources change with epoch. If all sources undergo the same degree of LE it is described 'pure luminosity evolution' (PLE). Alternatively in *density evolution* (DE) the co-moving space density of a population changes with epoch. If all sources undergo the same degree of density evolution it is described as 'pure density evolution' (PDE). A combination of luminosity and density evolution is of course possible. Previous analyses which attributed a single evolution history to *all* radio sources (*i.e.* combining the FRI and FRII populations into a single 'steep-spectrum' population) have concluded that neither PLE nor PDE are applicable (e.g. Wall, Pearson & Longair 1980) and instead successful descriptions of the data have always required a form of luminosity-dependent evolution.

Furthermore there are two popular forms of parametric evolution, applicable to both density and luminosity evolution, which may have some physical significance: (i) power-law evolution of the form  $(1+z)^\eta$ ,  $(1+z)^{-1}$  being the universal scale factor, and (ii) exponential evolution of the form  $\exp M\tau(z)$ ,  $\tau$  being the look-back time. Whilst power-law evolution was successfully applied to models for optically-selected QSOs (Boyle, Shanks & Peterson 1988), exponential evolution has been found to be more applicable for radio-selected samples, as it reproduces the strong cosmic evolution observed at relatively modest redshift (e.g. Doroshkevich, Longair & Zeldovich 1970).

### 3.2 Methodology

Our approach follows that of Wall, Pearson & Longair (1980) by which the local radio luminosity function is determined given a complete *luminosity distribution* and a chosen *evolution function*  $F$ . The evolution function  $F(P, z)$  modifies the local radio luminosity function,  $\rho_0$ , to give the radio luminosity function at any epoch  $z$ , *i.e.*  $\rho(P, z) = \rho_0(P)F(P, z)$ . This description is entirely general and can describe luminosity evolution, density evolution, or a mixture.

The steps in this process to a description of space density are:

*For each population in the source count:*

- (i) Compile the luminosity distribution  $N(P)$  from a complete flux-limited sample of identifications and redshifts.
- (ii) Choose an evolution function  $F(P, z)$ .
- (iii) Calculate the local radio luminosity function  $\rho_0(P)$ :

$$\rho_0(P)dP = \frac{N(P)dP}{\int_0^{z(S)} F(P, z)dV(z)} \quad (1)$$

so that the radio luminosity function  $\rho(P, z) = \rho_0(P)F(P, z)$  is then known at all redshifts.

- (iv) Calculate the contribution to the radio source count:

$$N(\geq S) = \int_0^{\infty} dP \int_0^{z(S)} \rho_0(P)F(P, z)dV(z) \quad (2)$$

where  $z(S)$  is the redshift at which a source of intrinsic radio power  $P$  contributes at flux density  $S$ . A redshift cut-off  $z_c$  may be imposed, beyond which  $F = 0$ . In practice the differential source count for the population is calculated, flux-binned for comparison purposes exactly as the observed count has been compiled.

*When the contributions from all populations have been found:*

- (v) Sum the single-population source counts to give the total predicted count. The predicted and observed differential source counts are compared and the evolution functions are adjusted, the process iterating from step (ii) until an acceptable fit to the observed count is obtained.

### 3.3 Determining the evolution functions $F(P, z)$

A suitable trial form for the evolution function can be determined from the  $\langle V/V_{max} \rangle$  statistic for a complete sample. The best sample available at low frequencies is the 3CRR sample at 178 MHz (Laing, Riley & Longair 1983 and more recently published data collated by R. Laing, private communication) as it is complete in terms of radio morphologies and redshifts.

- (i) **FRII Evolution.** A plot of  $V/V_{max}$  (Figure 2) for the 137 steep-spectrum FRII sources in 3CRR indicates that the highest radio power FRII sources have undergone far more evolution than the lower-power ones. Whilst  $\langle V/V_{max} \rangle = 0.664$  ( $\sigma=0.025$ ) for the 137 FRII sources, this value rises from 0.415 ( $\sigma=0.118$ ) at  $\log_{10}(P_{151 \text{ MHz}}) = 24.25$  to 0.807 ( $\sigma=0.052$ ) at  $\log_{10}(P_{151 \text{ MHz}}) = 28.25$ .

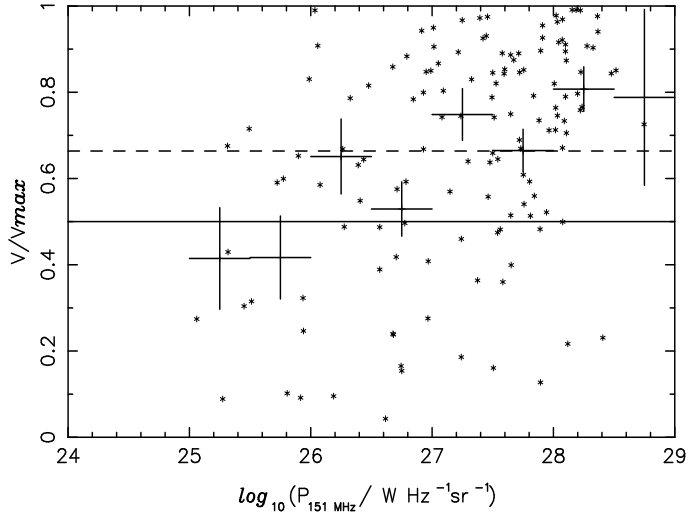


**Figure 2.**  $V/V_{max}$  values (\*) for the 137 steep-spectrum FRII sources in 3CRR.  $\langle V/V_{max} \rangle$  for the total sample is shown dashed.  $\langle V/V_{max} \rangle$  values for bins in  $\Delta \log_{10}(P_{151 \text{ MHz}}) = 0.5$  are shown as data points (+).

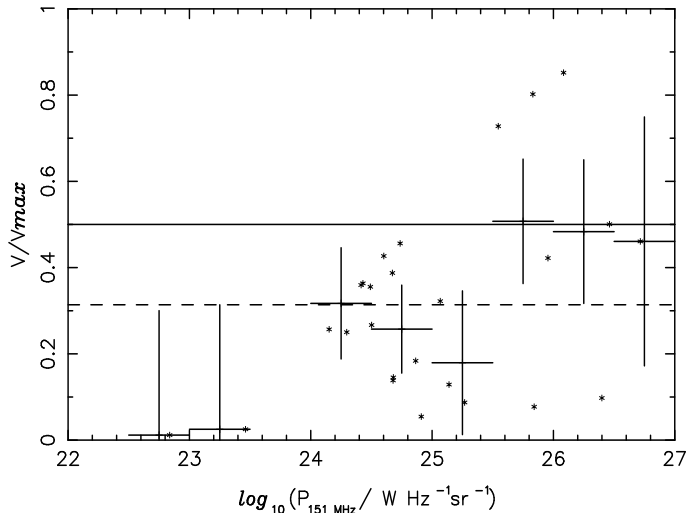


**Figure 3.**  $V/V_{max}$  values (\*) for the 26 steep-spectrum FRI sources in 3CRR.  $\langle V/V_{max} \rangle$  for the total sample is shown dashed.  $\langle V/V_{max} \rangle$  values for bins in  $\Delta \log_{10}(P_{151 \text{ MHz}}) = 0.5$  are shown as data points (+).

- (ii) **FRI Evolution.** The  $V/V_{max}$  statistic for the 26 FRI sources in 3CRR is shown in Figure 3. In contrast to the strong evolution indicated for the FRII population, the FRIs show little evidence of evolution, with  $\langle V/V_{max} \rangle = 0.314$  ( $\sigma=0.057$ ) for all 26 sources possibly reflecting some negative evolution. The highest-power FRI sources in 3CRR have a value of  $\langle V/V_{max} \rangle = 0.507$  ( $\sigma=0.144$ ) at  $\log_{10}(P_{151 \text{ MHz}}) = 25.75$ .

To model the luminosity dependence of the parent-source evolution we adopt exponential luminosity-dependent-density evolution (*cf* ‘model 4b’ of Wall, Pearson

& Longair 1980) such that the evolution function  $F(P, z)$  has the form

$$F(P, z) = \exp M(P) \tau(z) \quad (3)$$

where  $\tau(z)$  is the look-back time in units of the Hubble time. For Einstein-de-Sitter ( $\Omega=1$ ) geometry this is given by

$$\tau(z) = (1 - (1 + z)^{-1.5}). \quad (4)$$

Additionally we apply a redshift cutoff to the populations mirroring the observed behaviour of the powerful radio sources at high redshift (Shaver et al. 1996). The evolution function is modified such that the evolution peaks at  $z_c/2$  and declines to zero at the cut-off redshift  $z_c$ :

$$F = F(P, z) \text{ for } z \leq z_c/2,$$

$$F = F(P, z_c - z) \text{ for } z_c/2 < z \leq z_c \text{ and}$$

$$F = 0 \text{ for } z > z_c.$$

The evolution rate  $M$  is set between 0 and  $M_{max}$  dependent on radio power  $P$ :

$$M(P) = M_{max} \frac{\log_{10} P - \log_{10} P_1}{\log_{10} P_2 - \log_{10} P_1} \quad \text{for } P_1 \leq P \leq P_2,$$

$M(P) = 0$  for  $P < P_1$ , i.e. no evolution of radio sources of radio power less than  $P_1$ ,

and  $M(P) = M_{max}$  for  $P > P_2$ , i.e. sources of radio power greater than  $P_2$  undergo maximal evolution.

### 3.4 Determining the evolution

#### 3.4.1 Deriving the LRLF

Luminosity distributions were compiled for the powerful radio sources from the complete 3CRR sample, comprising 173 sources with  $S_{178 \text{ MHz}} \geq 10.9$  Jy. In this analysis the 10 flat-spectrum sources ( $\alpha_{178 \text{ MHz}}^{750 \text{ MHz}} > -0.5$ , where  $S \propto \nu^\alpha$ ) are excluded so the remainder are steep-spectrum sources, 'uncontaminated' by the effects of Doppler beaming.

The 178-MHz flux densities were translated to 151 MHz using a single spectral index  $\alpha_{151 \text{ MHz}}^{178 \text{ MHz}} = -0.75$ , the mean value for the 3CRR steep-spectrum sample. Separate luminosity distributions were compiled for the FRI and FRII steep-spectrum parent populations, there being 26 FRI and 137 FRII sources in the sample. The unbinned data were smoothed to give a master luminosity distribution for each population by convolving each of the unbinned luminosities with a Gaussian curve of unit area, varying  $\sigma$  until the sum of all contributions is smooth whilst preserving the 'real' features of the distribution. The binned and master luminosity distributions for the two populations are shown in Figure 4.

The local radio luminosity functions for the FRI and FRII populations are then determined from equation 1, using the evolution function described by equation 3. However, the scarcity of radio sources in the 3CRR sample with radio powers below  $\log_{10} P_{151 \text{ MHz}} = 10^{24} \text{ W Hz}^{-1} \text{ sr}^{-1}$  yields an incomplete LRLF at these radio powers. This incompleteness is resolved by incorporation of the LRLFs determined for (i) the 'local' E/S0 galaxies (Condon 1984) considering

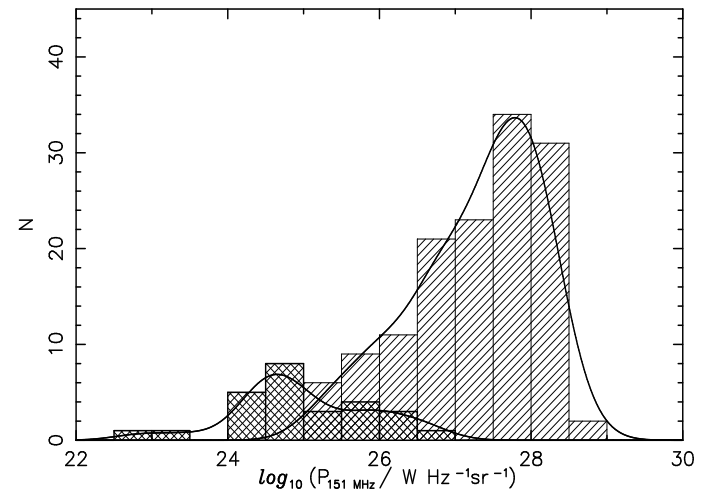


**Figure 4.** Luminosity distributions for the 26 FRI (cross-hatched) and 137 FRII (hatched) radio sources in 3CRR. The smoothed master luminosity distributions are over-plotted and were derived with  $\sigma=0.35$  in  $\log_{10}(P_{151 \text{ MHz}})$  as discussed in the text.

them as part of the FRI population, and (ii) the starburst galaxies, with the LRLF as derived by Rowan-Robinson et al. (1993) and the evolution function of Saunders et al. (1990). These starburst sources were folded into the space density analysis with the set evolution function

$$F_{star}(z) = \exp Q \tau(z)$$

with  $\tau(z)$ , the look-back time, as given in equation 4. The evolution function  $F_{star}$  describes pure luminosity evolution as follows:

$$Q = 3.1 \text{ for } 0 \leq z \leq 2,$$

$$F_{star}(z) = F_{star}(z=2) \text{ for } 2 < z \leq 5,$$

$$\text{and } F_{star}(z) = 0 \text{ for } z > 5.$$

The total local radio luminosity function is then the sum of the LRLFs for each of the three populations (FRI, FRII and starburst galaxies). The derived LRLF (Figure 5) shows that the transition between the FRI and FRII populations is gradual; the luminosity functions were tapered to avoid discontinuities, with the result that the space densities for low-power FRIIs ( $\log_{10} P_{151 \text{ MHz}} < 23.5$ ) and high-power FRIs ( $\log_{10} P_{151 \text{ MHz}} > 27.5$ ) are insignificant.

We find good agreement with other LRLFs determined independently. At the low-power end the total LRLF agrees well with those determined by Dunlop & Peacock (1990); Sadler, Jenkins & Kotanyi (1989); Auriemma et al. (1977). This agreement suggests that our FRI LRLF is reasonably well defined. This definition is important as low-power FRI sources are far more numerous locally than the higher-radio-power FRI found in the 3CRR sample, and at low flux densities their contribution is substantial.

The model FRI and FRII LRLFs from the Milne ver-

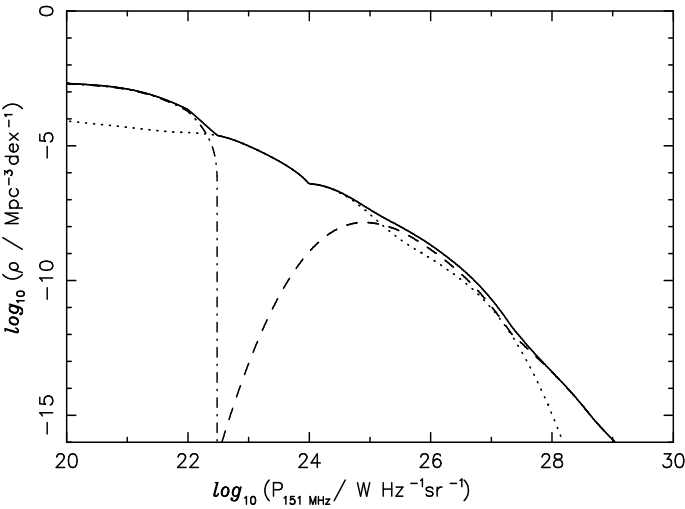


**Figure 5.** Derived LRLF at 151 MHz. The solid line is the total LRLF with constituent populations FRI (dotted), FRII (dashed) and starburst galaxies (dot-dashed).

sion of our successful model fit are in agreement with the results of Urry & Padovani (1995), expected as both analyses find little or no evolution of the FRI population. However, there is a major discrepancy between the two FRII LRLFs. Urry and Padovani adopted pure luminosity evolution for the FRII population, which predicts a high local space density of low-power FRIIs. According to Urry and Padovani's LRLF there should be similar local space densities of FRIs and FRIIs. Much smaller local space densities for FRIIs are observed; Ledlow & Owen (1996) find only 6% of FRIIs in a local survey of Abell clusters ( $z < 0.09$ ). However, overestimation of the LRLF for low-power FRIIs does not affect the analysis performed by Urry and Padovani which concentrates on fitting the RLF for the high-power quasar population.

#### 3.4.2 Fitting the 151-MHz source count

The parameters in the evolution functions for FRI and FRII sources were optimized by performing a  $\chi^2$ -minimization between the observed source count at 151 MHz and the total count predicted by the differentially-evolving RLF. The minimization was achieved using the *AMOEBA* downhill simplex method in multi-dimensions (Press et al. 1992). The unique set of evolution parameters thus derived for each parent population is shown in Table 2.

The 151-MHz source count used in this comparison (Figure 6) consists of the count from the 6C survey (Hales, Baldwin & Warner 1988) and the count from the 3CR survey from the 3CRR catalogue at 178 MHz (Laing, Riley & Longair 1983), transposed to 151 MHz using a single spectral index of  $-0.75$ .

The set of parameters given in Table 3 provides a good fit to the observed source count. This fit has *strong* cosmic evolution of the FRII population coupled with *no* evolution of the FRI population. The fit to the differential count is shown in Figure 6. For the most powerful FRII sources this

**Table 2.** Evolution functions used in the source count fit.

Population	Evolution function	Fixed evolution ?	Evolution parameters
FRI	exp LDDE	No	$M_{max}, z_c, P_1, P_2$
FRII	exp LDDE	No	$M_{max}, z_c, P_1, P_2$
starburst	exp PLE	Yes	$Q=3.1$

**Table 3.** Fitted evolution parameter values.

Population	Evolution parameter values	Chi-square test
FRI	$M_{max}=0.0, z_c=5.0$ ( $P_1$ & $P_2$ not used given $M_{max}=0.0$ )	$\chi^2_{min}$
FRII	$M_{max}=10.93, z_c=5.62,$ $P_1=25.44, P_2=27.34$	$\nu^\dagger$
	<i>best fit</i>	30.73 33

$^\dagger$  degrees of freedom.

model predicts a space density enhancement at  $z=2.8$  of  $> 10^4$  that of the local space density (Figure 7). That the FRI population undergoes little or no evolution is a *requirement* of the 151-MHz source count fit: any significant evolution produces an excess of faint sources, in disagreement with the decline of the differential source count towards lower flux densities. The successful fit also indicates a redshift cut-off in the FRII population, with the fit with  $z_c=5.62$  superior to that with  $z_c = \infty$  at the 99.9% level of significance. As a result the model reproduces the 'quasar epoch', reflected as a peak in the FRII space density (Figure 7) around  $z=2-3$ , as seen for powerful flat-spectrum quasars (Shaver et al. 1996).

## 4 RADIO-SOURCE BEAMING IN THE UNIFIED SCHEME

According to the dual-population unified scheme, flat-spectrum quasars and BL Lac-type sources are the steep-spectrum FRII and FRI sources aligned so that radio axes are close to our line-of-sight. The result is that the flat-spectrum emission from the approaching radio jet<sup>†</sup> is Doppler-boosted or 'beamed'. This Doppler boosting can result in the jet emission dominating the extended lobe emission.

<sup>†</sup> It is the *base* of the approaching jet which is flat-spectrum. Alternative scenarios are that the relativistic emission is from (i) the stationary core of the radio source which is optically thick at the observing frequency or (ii) synchrotron plasma emanating from the central object. All three scenarios in agreement with the results here.

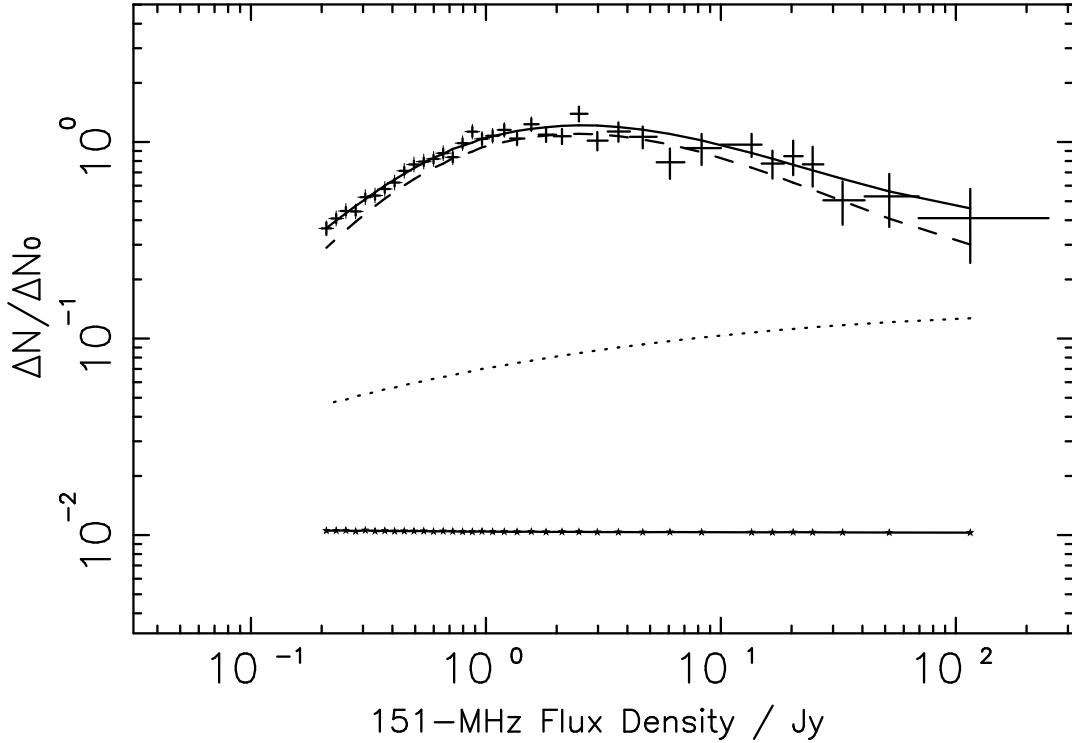


**Figure 6.** Source count fit at 151 MHz. Data points represent the observed differential source count at 151 MHz constructed as described in the text. The model produces contributions from the three populations, the FRII sources (dashed), the FRI sources (dotted) and the starburst galaxies ( $\star$ ). The total model count is shown as a solid line. All counts are shown in relative differential form with  $N_0 = 2400(S_{151 \text{ MHz}})^{-1.5} \text{ sr}^{-1}$ .

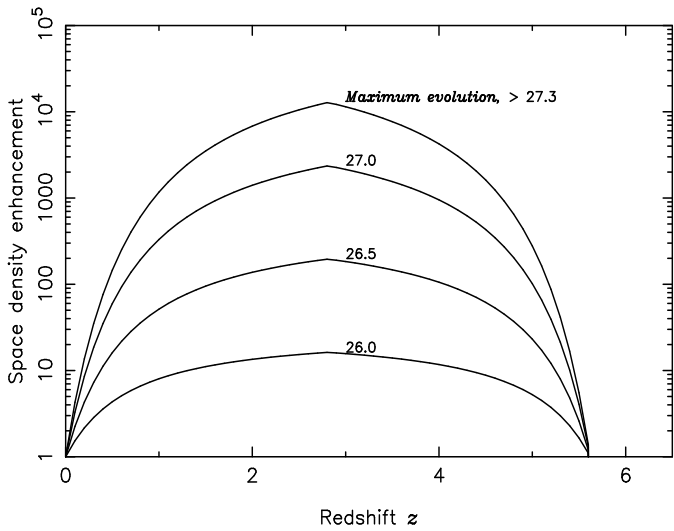


**Figure 7.** Space density enhancements as determined from optimized model parameters for a range of  $\log_{10}(P_{151 \text{ MHz}})$  values as shown.

Having derived the space density and its epoch-dependence for the parent populations, the low-frequency counts and identification statistics are satisfied. Translating the count of these steep-spectrum objects to 5 GHz reveals the shortfall at high flux densities in particular which must

be there: no flat-spectrum sources have yet been included and such sources constitute more than half of those found in cm-wavelength surveys. To provide this contribution we ‘beam’ the parent populations, orienting objects randomly to mimic the effects of the Doppler-enhanced radiation when lines-of-sight and ejection axes come into close coincidence. The parameters required to describe the beamed emission for any source are the spectral index of the core/jet emission, the Lorentz factor  $\gamma = (\sqrt{1 + (v/c)^2})^{-1}$  for the bulk motion in the jets, and the the intrinsic ratio  $R_c$  of core-to-lobe radio luminosity. We adopt a simple model of the Doppler beaming for each of the two populations, with the beaming parameters varied to produce the best statistical fit to the 5-GHz source count.

#### 4.1 The Doppler beaming parameters

We chose to model the Doppler beaming of the FRI and FRII populations with a range of intrinsic core-to-extended flux ratios (distributed normally about a median value) together with a single Lorentz factor for each parent population. There is an additional complication for the FRI population, for which the intrinsic ratio for the is a function of radio power with significant scatter about a median value (de Ruiter, Parma & Fanti 1990). In contrast, there is little evidence that the ratio correlates with radio power for the FRII population. Figure 8 shows the observed ratio for 47 high-excitation FRII galaxies from the 3CRR sample. The median ratio appears uncorrelated to total radio power, with

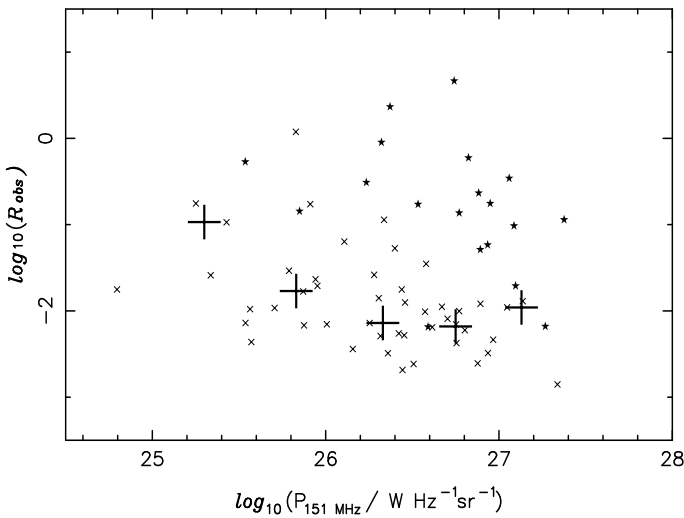


**Figure 8.** Observed core-to-extended flux ratios,  $R_{obs}$ , for high-excitation FRII sources in 3CRR, 47 galaxies ( $\times$ ) and 19 quasars ( $*$ ). Median  $R_{obs}$  values for the galaxies, *i.e.* those sources which are unbiased by Doppler beaming are shown as (+). From data compiled by R Laing.

a significant scatter around the median values. The same result has been seen (Morganti et al. 1997) in narrow-line radio galaxies from the 2-Jy sample (Wall & Peacock 1985).

For the FRI population we adopt the following function from the observed ratio for B2 galaxies (de Ruiter, Parma & Fanti 1990):

$$\log_{10} R_{med} = -0.55 \log_{10}(P_{151 \text{ MHz}}) + 10.78.$$

Therefore for the FRII population we reflect the observed values of the intrinsic ratio  $R_c$  by simply distributing it normally about a single median value  $R_{med}$ , with  $\sigma = 0.45 R_{med}$ .

## 4.2 Modelling the beamed products

The FRI and FRII populations give rise to beamed and unbeamed sources with the *observed* core-to-extended flux ratio,  $R_{obs}$ , determining whether a particular source is observed as flat- or steep-spectrum (Figure 9):

(i) A single spectral index,  $\alpha_{151 \text{ MHz}}^{5 \text{ GHz}} = -0.75$  is applied to the 151-MHz flux density to determine the flux density of the steep-spectrum contribution at 5 GHz. This represents the emission from the extended lobes of the source. The value of  $-0.75$  is adopted as it is the mean spectral index of the steep-spectrum 3CRR sources between 178 MHz and 750 MHz (Laing & Peacock 1980). We extrapolate this index to 5 GHz as there is no evidence that the spectrum of the steep-spectrum components in 3CRR steepens significantly between 178 MHz and 2.7 GHz (Laing & Peacock 1980). This steep-spectrum component flux density,  $S_{5 \text{ GHz},steep}$ , is

$$S_{5 \text{ GHz},steep} = S_{151 \text{ MHz}} \cdot (5000/151)^{-0.75},$$

shown as line A to B in Figure 9.

(ii) The emission from the flat-spectrum core of the source is calculated assuming that the source comprises a pair of oppositely-directed relativistic jets of bulk plasma velocity  $\beta c$ . The ejection axis of these jets is aligned at some random angle  $\theta$  ( $0^\circ \leq \theta \leq 90^\circ$ ) to our line-of-sight. The observed core-to-extended flux ratio,  $R_{obs}$ , determines the degree of beaming observed as follows:

$$R_{obs} = R_c \Delta$$

where  $\Delta$  is the sum of the Doppler enhancement from the forward- and counter-jets of the source:

$$\Delta = \delta_f^p + \delta_c^p.$$

with the Doppler factor for the forward-jet,  $\delta_f$ , as

$$\delta_f = (\gamma(1 - \beta \cos \theta))^{-1}$$

and for the counter-jet,  $\delta_c$ , as

$$\delta_c = (\gamma(1 + \beta \cos \theta))^{-1}$$

where  $\beta = v/c = (1 - \gamma^{-2})^{1/2}$ .

For radio emission comprising continuously-ejected plasma,  $p = 2 - \alpha_{flat}$ . We adopt a value for the spectral index of the core emission,  $\alpha_{flat}$ , of 0.0 as this is the mean spectral index  $\alpha_{408 \text{ MHz}}^{1.4 \text{ GHz}}$  of the core components of the B2 sources (de Ruiter, Parma & Fanti 1990).

Therefore the observed core-to-extended flux ratio is given by

$$R_{obs} = R_c ((\gamma(1 - \beta \cos \theta))^{-2} + (\gamma(1 + \beta \cos \theta))^{-2}).$$

The flux density of the beamed contribution,  $S_{5 \text{ GHz},flat}$ , is represented by line B to C in Figure 9 and is simply related to the steep-spectrum flux density by  $S_{5 \text{ GHz}} = R_{obs} \cdot S_{5 \text{ GHz},steep}$ .

(iii) A source is counted as ‘flat-spectrum’ for values of  $R_{obs}$  large enough such that  $\alpha_{2.7 \text{ GHz}}^{5 \text{ GHz}} \geq -0.5$ . This determines the value of  $R_{min}$ , the lowest  $R_{obs}$  value at which a source is counted as flat-spectrum, as follows:

The spectral index between 2.7 GHz and 5 GHz is given by

$$\alpha_{2.7 \text{ GHz}}^{5 \text{ GHz}} = \frac{\log_{10} \frac{S_{5 \text{ GHz},total}}{S_{2.7 \text{ GHz},total}}}{\log_{10} \frac{\nu_{5 \text{ GHz}}}{\nu_{2.7 \text{ GHz}}}}.$$

For  $\alpha_{flat}=0.0$  the flat-spectrum components have the same flux density at 2.7 GHz and 5 GHz, *i.e.*  $S_{2.7 \text{ GHz},flat} = S_{5 \text{ GHz},flat}$  and for  $\alpha_{steep}=-0.75$  the steep-spectrum components at 2.7 GHz and 5 GHz are related as  $S_{2.7 \text{ GHz},steep} = 1.6 S_{5 \text{ GHz},steep}$ . Thus we determine  $R_{min}$  as having the value of 0.66.

The largest angle between the jet and the line of sight for the source to appear flat-spectrum occurs at the the critical angle  $\theta_c$  when  $R_{obs} = R_{min}$ . Thus  $\theta_c = \delta_{min} = \delta(\theta_c)$  so that  $\theta_c$  is determinable from

$$\cos(\theta_c) = \frac{1}{\beta} - \frac{1}{\beta\gamma} \left( \frac{R_c}{R_{min}} \right)^{p-1}, \quad (5)$$

assuming that the beaming due to the counter-jet is negligible. In fact our successful model finds that  $\theta_c < 10^\circ$  and the assumption is justified.

Thus the only unknown parameters in the 5-GHz source count fit are values for  $\gamma$  and  $R_{med}$  for each of the FRI and FRII populations.

### 4.3 Fitting the 5-GHz source count

The 5-GHz source count is constructed from survey data as detailed in Table 4 and is well defined across a wide flux-density range. At 5 GHz, the beamed products of the FRI and FRII sources make a highly significant contribution to the source count; for flux densities above 0.5 Jy, some 55% of sources are ‘flat-spectrum’ Pauliny-Toth et al. (1978).

To define the populations in accordance with our earlier discussion of the FRII beamed products, we split the FRII parent sources into high- and low-excitation types using a simple linear function of  $\log_{10}(P_{151 \text{ MHz}})$  as suggested by Laing et al. (1994) and Barthel (1994). The fraction of low-excitation FRIIs was set at 50% at  $\log_{10} P_{151 \text{ MHz}} = 25.0$ , declining to zero at  $\log_{10} P_{151 \text{ MHz}} = 27.0$ .

The source count fit was carried out as for the 151-MHz count, this time incorporating the beamed products of the FRI and FRII sources by randomly aligning the sources with respect to our line-of-sight. The source alignment angle,  $\theta$ , for each of the FRI and FRII contributions was generated using NAG pseudo-random number routines. The best-fit beaming parameters were determined again using the *AMOEBA* downhill simplex method, minimizing  $\chi^2$  evaluated between the observed and model source counts at 5 GHz.

A good fit to the 5-GHz source count was found for the parameter values given in Table 6.

The observed source count and the count calculated for the optimum fit are shown in Figure 10. Here the sub-populations contributing to the count are split into their beamed and unbeamed products as detailed in Table 5. The contribution from the beamed sources peaks at high flux densities ( $0.1 < S_{5 \text{ GHz}} < 10$  Jy), broadening the ‘evolution bulge’ of the count. Thus the unification scheme provides a straightforward explanation of *why* the source-count ‘plateau’ widens with survey frequency. It is the Doppler-beaming of the FRII population which has the primary impact in this respect. The combination of zero evolution with milder Doppler beaming for the FRI population results in a monotonically-decreasing count of beamed and unbeamed FRIs throughout the flux density range as shown.

## 5 TESTING THE MODEL

The substantial predictive power of the model provides direct tests of the dual-population unified scheme.

### 5.1 The beaming models

**Table 6.** Fitted beaming parameter values.

Population	parameter values	Chi-square test	
		$\chi^2$	$\nu^\dagger$
FRII	$\gamma=8.5, R_{med}=0.01$ $\theta_c(R_{med})=7.1$		
FRI	$\gamma=15.0$ $R_{med} \propto P_{151 \text{ MHz}}^{-0.55}$		
		best fit	32.98
			25

$^\dagger$  degrees of freedom.

#### 5.1.1 Jet speeds; values of the Lorentz factor $\gamma$

The single most successful aspect of the model is that values of  $\gamma$  determined from the optimization process agree with those determined from estimates made from (i) VLBI observations of superluminal sources and (ii) synchrotron self-Compton models for the observed and predicted X-ray flux.

VLBI studies of superluminal sources measure the apparent velocities of recognisable features in radio sources. Results from a large ( $> 100$ ) sample of superluminal sources show that, assuming that the bulk and pattern speeds are the same,  $\gamma_{min} \sim 4$  are commonly found although there is a wide spread of values from  $2 \leq \gamma \leq 20$  (Vermeulen 1995).

The synchrotron self-Compton model estimates the Doppler beaming from the observed and predicted X-ray flux densities of radio sources. For a sample of  $\sim 100$  sources a *lower* limit for the bulk Lorentz factor of  $\sim 10$  is found with a viewing angle  $\sim 8^\circ$  for all superluminal sources. This analysis also indicates that the core-to-extended flux ratio has a significant scatter (Ghisellini et al. 1993).

In addition to the above,  $\gamma \sim 10$  successfully accounts for the non-detection of a counter-jet in highly-aligned objects such as 3C 273 (Davis, Unwin & Muxlow 1991).

#### 5.1.2 The observed core-flux : extended-flux ratio

The observed core-to-extended flux ratios,  $R_{obs}$ , span a wide range of values. The most lobe-dominated sources, those unaffected by Doppler beaming, have ratios as low as  $R_{obs} \sim 10^{-5}$  (e.g. OD-159 from the 2-Jy sample, Morganti, Killeen & Tadhunter 1993). In contrast the most core-dominated sources are heavily Doppler-beamed and can have  $R_{obs} \sim 10^3$  (e.g. PKS B0400+258, Murphy, Browne & Perley 1993).

Our assumption of a normal distribution for  $R_c$  about  $R_{med}$  results in a wide range of  $R_{obs}$  for both FRI and FRII beamed products (Figures 11 and 12), and provides a smooth transition between the parent objects and their beamed sources. The  $R_{obs}$  values for BL Lac-type sources are predicted to extend to higher values due to the large range of intrinsic  $R_c$  values. The limited data in complete samples appropriate for comparison are in approximate agreement.

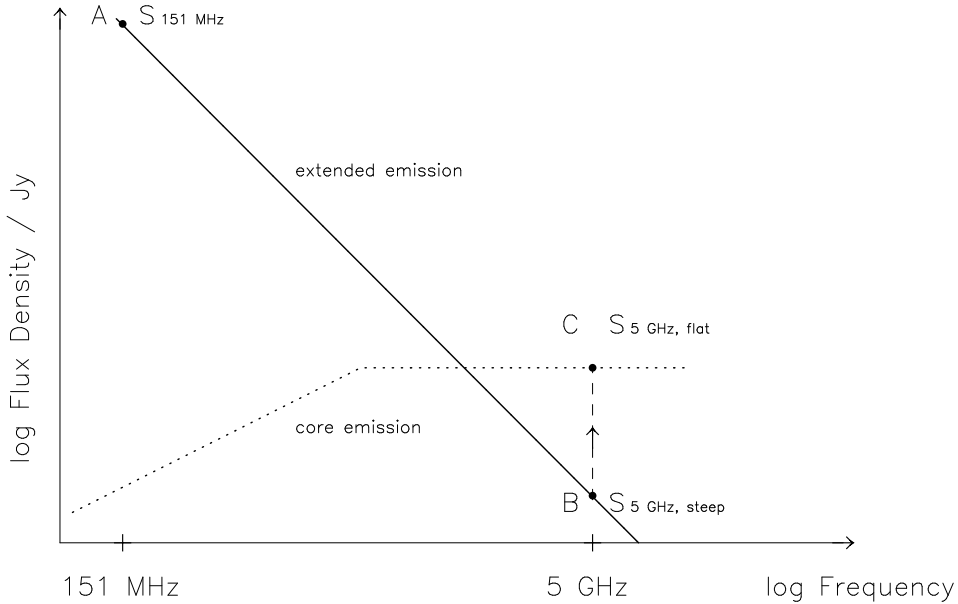


**Figure 9.** Modelling the flat- and steep-spectrum components of the FRI and FRII sources at 5 GHz. The contribution from the steep-spectrum component at 151 MHz (A) is transposed to 5 GHz (B) using  $\alpha_{151 \text{ MHz}}^{5 \text{ GHz}} = -0.75$  (solid line). If the radio axis lies close to the line-of-sight ( $\theta \leq \theta_c$ ) the core emission (dotted) dominates and the source appears ‘flat-spectrum’; the total flux density of the source is  $S_{5 \text{ GHz}, \text{steep}} + S_{5 \text{ GHz}, \text{flat}}$ .

**Table 4.** 5-GHz source count data.

Flux density range $S_{5 \text{ GHz}}$	Survey instrument(s)	Survey name	Reference
10 Jy - 100 Jy	NRAO + MPIfR	strong sources	Kühr, Pauliny-Toth & Nauber (1981)
1.5 Jy - 10 Jy	Green Bank 91m	87 GB	Gregory & Condon (1991)
0.5 Jy - 1.3 Jy	NRAO + MPIfR	S4	Pauliny-Toth et al. (1978)
67 mJy - 0.5 Jy	NRAO 300ft	6cm survey	Davis (1971)
10 mJy - 55 mJy	MPIfR	deep selected regions	Pauliny-Toth, Steppe & Witzel (1980)
1.5 mJy - 8.5 mJy	VLA	E/S0 galaxy	Wrobel & Krause (1990)
1.36 mJy - 6.00 mJy	VLA	Lynx-2 area	Donnelly, Partridge & Windhorst (1987)
16 $\mu$ Jy - 60 $\mu$ Jy	VLA	DEEPS2	Fomalont et al. (1991)

## 5.2 Multi-frequency source counts

Figure 13 shows the observed differential source counts at a wide range of radio frequencies together with the predictions of counts from the model. The model successfully reproduces these source counts, qualitatively at least. There are quantitative differences, most notably the excess in the prediction at low flux densities for 1.4 GHz. The most probable explanation is that our simple model of the local luminosity function overestimates the space density for powers below  $\log_{10}(P_{151 \text{ MHz}}) \sim 24.0$ .

## 5.3 Core-dominated and broad-line fractions

Figure 14 shows the population mix as predicted by the model as a function of 5-GHz flux density. The striking feature is the change in dominant population moving from high flux densities (high-excitation FRII radio galaxies and quasars) to low flux densities (FRI radio galaxies, BL Lac-

type sources and - eventually - starburst galaxies). The domination of the high-excitation FRII sources at high flux densities produces a pronounced peak in the quasar population between 0.5 and 10 Jy; the decline in quasar fraction towards lower flux densities is in close agreement with observation (Figure 15), as discussed by Wall & Jackson (1997).

The change in fraction of broad-line sources as a function of flux density agrees with the best available determinations at 408 MHz (Figure 5 of Wall & Jackson (1997)). Such a change is evidence for the unified scheme rather than evidence against it as was suggested by Singal (1996). Despite its relative simplicity, the dual-population scheme shows that tests of unification dealing with broad-brush proportions of broad-line objects or flat-spectrum objects are far too simplistic; the mix of sub-populations selected in each sample must be considered. There must be similar reservations over elementary tests based on size discrimination (e.g. Kapahi et al. 1996).

**Table 5.** Radio source types at 5 GHz.

Ref <sup>#</sup>	Source population/evolution/ beamed & unbeamed products	Beamed at 5 GHz ?	Radio spectrum $\alpha_{2.7 \text{ GHz}}^{5 \text{ GHz}}$
<i>FRII sources</i>			
	tapered exp LDDE, $F(P, z) = \exp M(P)\tau(z)$ <i>evolution parameters as determined in section 3</i>		
1	High-excitation radio galaxies & quasars (class A)	no	steep
2	Quasars	yes	'flat'
3	Low-excitation radio galaxies (class B)	no	steep
4	BL-Lac type objects	yes	'flat'
<i>FRI sources</i>			
	<i>non-evolving as determined in section 3</i>		
5	FRI radio galaxies (class B)	no	steep
6	BL-Lac type objects	yes	'flat'
<i>low-power</i>			
	exp PLE, $F(z) = \exp Q\tau(z)$ <i>PLE as described in section 3</i>		
7	starburst galaxies	no	steep

<sup>#</sup> These numbers are used to reference the source types in Figures 10 to 17.

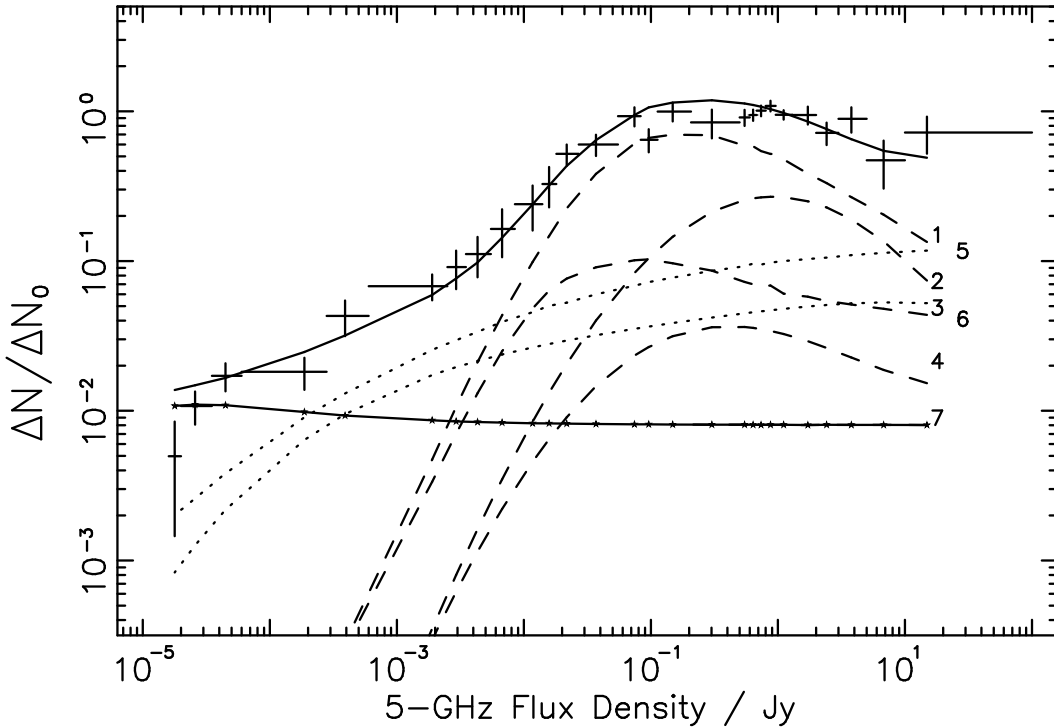


**Figure 10.** Source count fit at 5 GHz. Data points represent the differential source count at 5 GHz from data given in Table 4. The model produces contributions from seven source types as described in Table 5. All counts are shown in relative differential form with  $N_0 = 60(S_{5 \text{ GHz}})^{-1.5} \text{ sr}^{-1}$ .

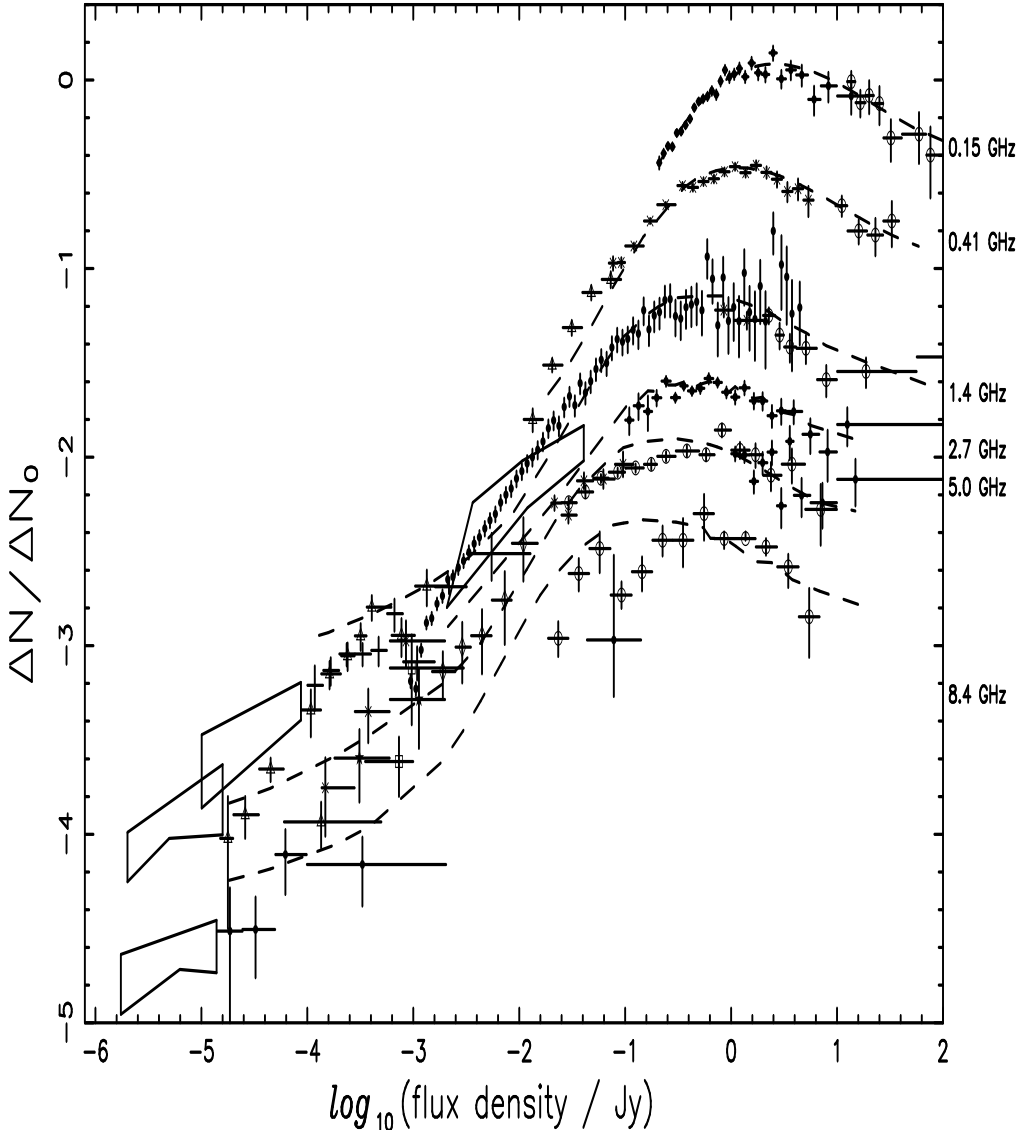


**Figure 13.** Observed source counts at six frequencies with data points from surveys as given in Wall (1994) and the addition of the VLA FIRST survey source-count points  $1 \text{ mJy} \leq S_{1.4 \text{ GHz}} \leq 1 \text{ Jy}$  (Becker, White & Helfand 1995). The predicted model counts are shown dashed. All counts are in relative differential form  $\Delta N / \Delta N_0$ , where  $\Delta N$  is the number of sources per sterad with flux density  $S_\nu$  between  $S_2$  and  $S_1$  and  $N_0 = K_\nu S_\nu^{-1.5}$ , the number of sources expected in a uniformly-filled Euclidean universe. The values of  $K_\nu$  are 2400, 2730, 3618, 4247, 5677 and 3738 respectively for the six frequencies shown. The horizontal range bars show the flux-density bin width  $S_2$  to  $S_1$ , and the error bars represent  $\sqrt{N}$  uncertainties. Polygons show the count estimates from  $P(D)$  (background-deflection) analyses.

#### 5.4 The redshift distribution of flat-spectrum quasars

A single sub-population redshift distribution,  $N(z)$ , provides a potent test of the model. The flat-spectrum sample of Shaver et al. (1996) comprises 444 sources, all of which are identified. Of these, 358 quasar redshifts were available to us. The sample is moderately complete to  $S_{2.7 \text{ GHz}} = 0.25 \text{ Jy}$  although a substantial proportion of the sample is limited to  $S_{2.7 \text{ GHz}} = 0.6 \text{ Jy}$ . All sources were selected as flat-spectrum, with  $\alpha_{2.7 \text{ GHz}}^5 \geq -0.4$  ( $S \propto \nu^\alpha$ ). The redshift distribution for the observed sample of 358 quasars is shown in Figure 16, along with the model prediction for an equivalent *complete* flux-limited sample ( $S_{2.7 \text{ GHz}} \geq 0.5 \text{ Jy}$ ). The model success-

fully replicates the observed  $N(z)$  for the largest sample of spectroscopically-identified quasars available. It should be emphasized that these data are completely independent of the (low-frequency) data used to construct the model.

#### 5.5 Radio surveys to mJy flux-density levels

The new, large-area radio surveys (*i.e.* FIRST, NVSS, WENSS & SUMSS) reach mJy flux-density levels and will yield samples forming the basis of future direct tests of the dual-population model.

Figure 17 shows the predicted integral population mix as a function of 1.4-GHz flux density. The dominant populations in the range  $1 \leq S_{1.4 \text{ GHz}} < 100 \text{ mJy}$  differ sub-

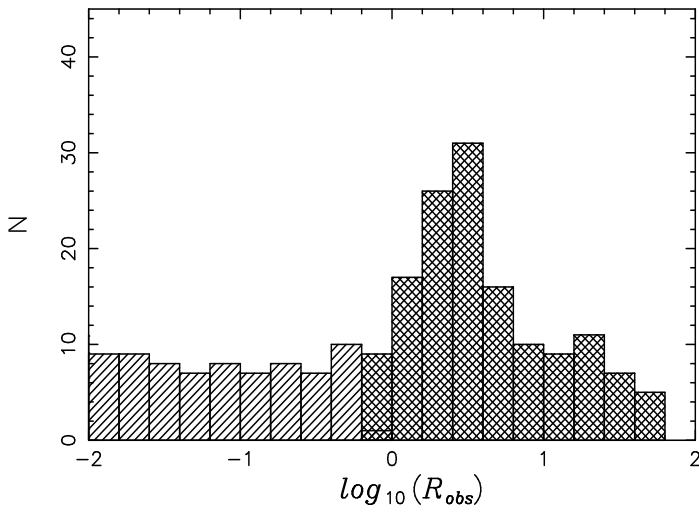


**Figure 11.** Model  $R_{obs}$  distribution for the flat-spectrum BL-Lac type sources (cross-hatched), plus steep-spectrum FRI and low-excitation FRII sources (hatched), over 1 sterad with  $S_{5\text{ GHz}} \geq 0.1$  Jy.

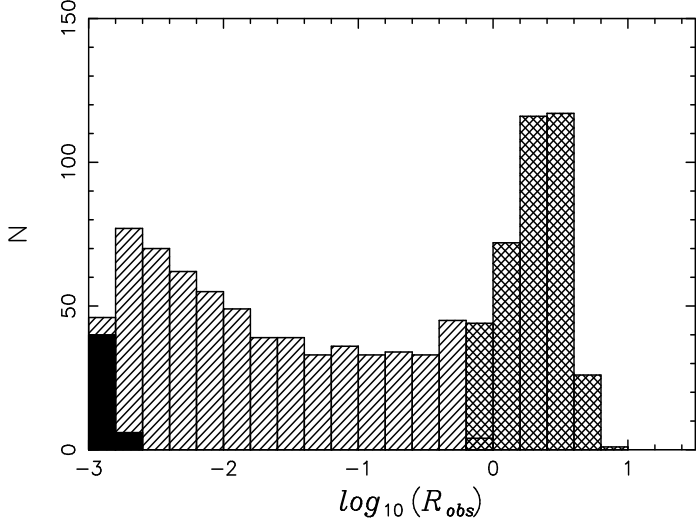


**Figure 12.** Model  $R_{obs}$  distribution for (i) flat-spectrum quasars (hatched), (ii) steep-spectrum quasars and broad-line radio galaxies, *i.e.* high-excitation FRIIs with radio axes within  $50^\circ$  of the line-of-sight (hatched), and (iii) narrow-line radio galaxies, high-excitation FRIIs with radio axes lying  $> 50^\circ$  from the line-of-sight (solid fill), over 1 sterad and with  $S_{5\text{ GHz}} \geq 0.1$  Jy.

stantially from those at higher flux density. A direct consequence of the dual-population model with its strong differential evolution is the dramatic decline in prominence of the high-excitation FRIIs (and hence broad-line objects) toward 1 mJy.

This change in population with flux density likewise has major influence on the redshift distribution of sources, as Table 7 illustrates. At  $0.1 \leq S_{1.4\text{ GHz}} < 100$  Jy the population is predominantly FRII sources at high redshift, while

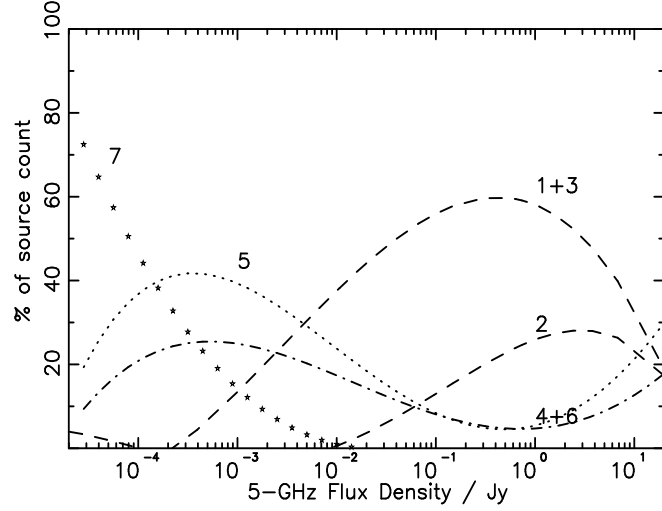


**Figure 14.** The predicted population mix at 5 GHz, with populations as given in Table 5.

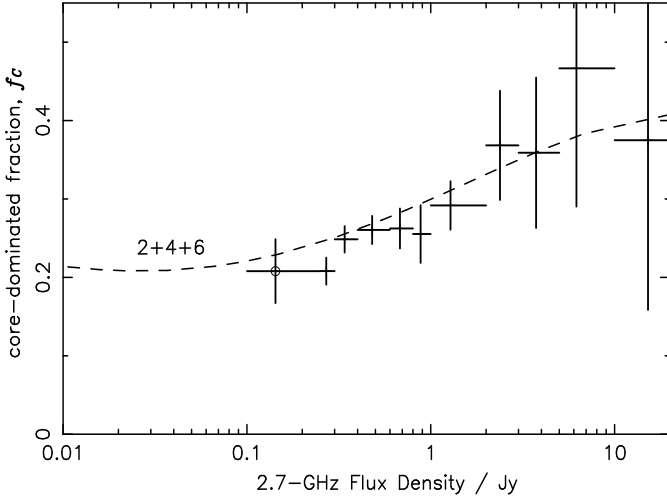


**Figure 15.** Core-dominated fractions at 2.7 GHz. The dashed line is the model prediction of core-dominated sources (BL Lacs plus quasars). The data points are derived from two samples discussed in detail by Wall & Jackson (1997), section 3.1: PKSCAT90 (+) with  $S_{2.7\text{ GHz}} \geq 0.25$  Jy and PSR (o) with  $0.10 \leq S_{2.7\text{ GHz}} < 0.25$  Jy. The error in  $f_C$  is  $\sqrt{N_q} / (\text{bin total})$ .

a very much more local distribution of sources appears at  $1 \leq S_{1.4\text{ GHz}} < 100$  mJy as the low-power FRIIs and eventually the starburst galaxies rise to prominence.

Figure 18 shows a comparison between  $N(z)$  distributions for a flux density range  $1 \leq S_{1.4\text{ GHz}} < 100$  mJy. The striking differences between our model prediction and the average  $N(z)$  model of Dunlop & Peacock (1990) are (*i*) the sharp spike at  $z \sim 0.1$  due to the starburst galaxies in our model, a population not included in the Dunlop & Peacock analysis, (*ii*) the lower median redshift distribution of sources in the prediction of the current model, due to

**Table 7.** Population mix at 1.4 GHz.

Flux density range	FRII high-excitation		FRII low-excitation		— FRI —		Starburst galaxies (7)
	BL & NLRGs (1)	Quasars (2)	RGs (3)	BL Lac (4)	RGs (5)	BL Lac (6)	
$S_{1.4\text{ GHz}} > 100 \text{ mJy}$	59%	15%	10%	4%	7%	4%	1%
$1 \leq S_{1.4\text{ GHz}} \leq 100 \text{ mJy}$	7%	1%	4%	-	38%	30%	20%

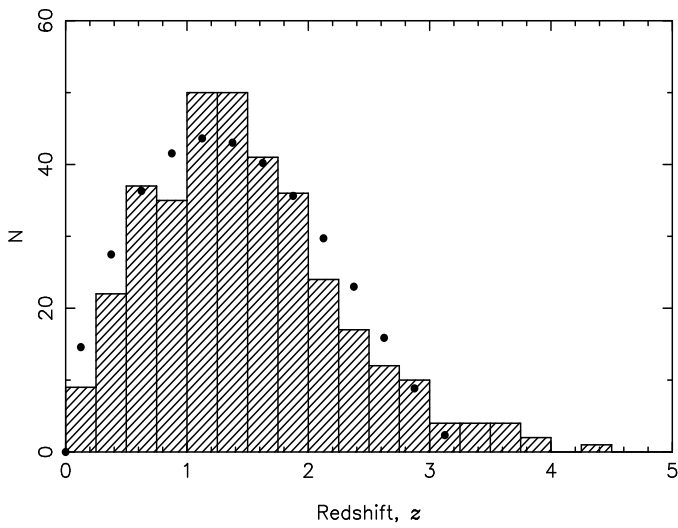


**Figure 16.** The redshift distribution for 358 flat-spectrum quasars from Shaver et al. (1996), shown with the model prediction for 358 quasars selected with  $\alpha_{2.7\text{ GHz}}^5 \geq -0.4$  and  $S_{2.7\text{ GHz}} \geq 0.5$  Jy.

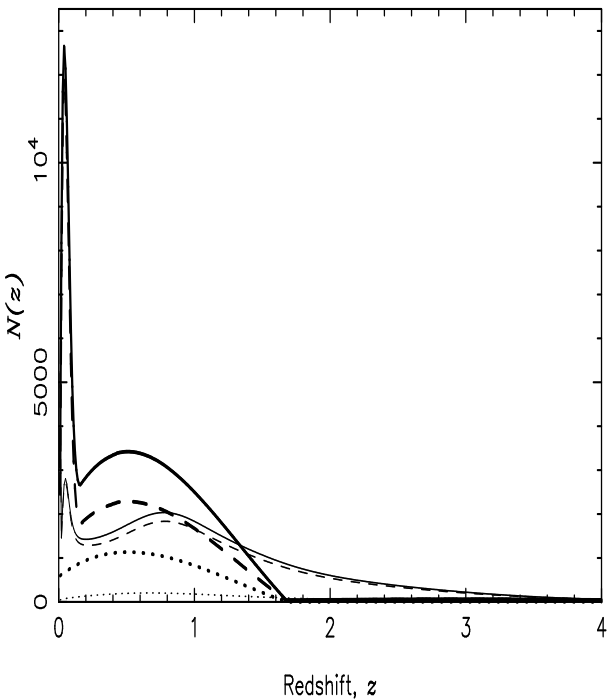


**Figure 18.** The predicted  $N(z)$  (per  $0.01z$  per sterad) for sources with  $1 \leq S_{1.4\text{ GHz}} < 100 \text{ mJy}$ . Models are from Dunlop & Peacock (1990) (average of their models 1-7), shown as thin lines, and this paper, shown as thick lines. Legend: ... flat-spectrum sources, - - steep-spectrum sources and solid line total of all sources.

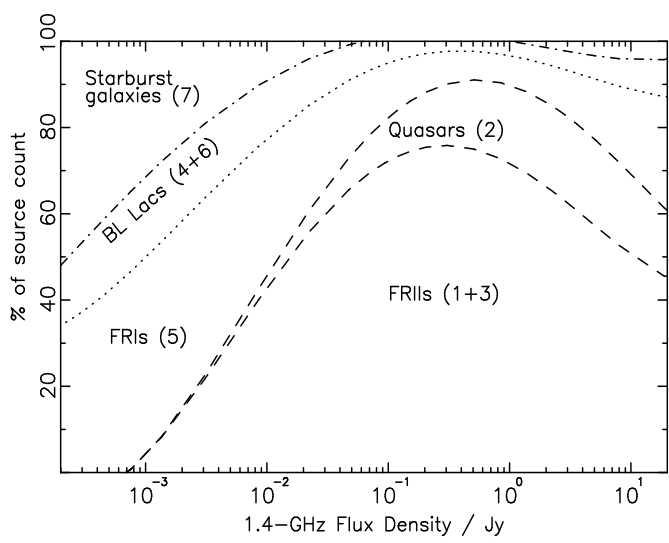


**Figure 17.** The predicted (integral) population mix at 1.4 GHz with the populations as described in Table 5.

the dominance of the unevolving FRI sources within this flux density range, and (iii) the greater prominence of flat-spectrum sources in our model, the beamed products of the low-power FRI sources.

Although the model predicts unequivocal  $N(z)$  and population mix, *e.g.* for flux densities in the range  $1 < S_{1.4\text{ GHz}} < 100 \text{ mJy}$ , it has been developed from consideration of *total* source counts at high and low frequencies, but *population mix* only at low frequencies and high flux densities,  $S_{178\text{ MHz}} > 10.9$  Jy. Complete samples (with redshifts) at the mJy level offer substantial scope for improvement or refinement of the parameters. For example, the sample at  $S_{2.7\text{ GHz}} = 0.3$  mJy of Gruppioni et al. (1997) contains more broad-line objects than predicted. If confirmed, this suggests that we have overestimated the the FRI LRLF at low pow-

ers, a possibility already suggested in §5.2. Tapering off the FRI LRLF more rapidly at its higher radio powers would require a compensatory broadening of the FRII LRLF, resulting in an increased proportion of FRII objects at sub-mJy levels.

## 6 CONCLUSIONS

We have described a paradigm in which evolution of extragalactic radio sources is delineated for populations which are physically related through orientation-dependent effects. The dual-population scheme is based on the premise that the two parent populations are radio galaxies of FRI and FRII morphologies, with distinctly different evolutions which we have determined from analysis of counts and identification data at low frequencies. The fundamental assumption is that all FRII and FRI radio galaxies have radio lobes fed with relativistic beams. The beaming models by which these parent objects appear as the quasars or BL Lac objects when lines-of-sight coincide closely with radio axes were then developed by considering the high-frequency counts and identifications, dominated by these beamed products.

The model provides agreement with source-counts and with identification and redshift data at high flux densities and at both high and low frequencies. It provides a natural explanation of the change in shape of source counts with frequency. Furthermore, such a unified scheme provides a natural explanation of why steep-spectrum sources show more pronounced cosmological evolution than do beamed (flat-spectrum) sources of the same (apparent) power (Dunlop & Peacock 1990), a result anticipated by Scheuer & Readhead (1979).

One of the clearest successes of the model is that the beam speeds derived from statistics of counts and identifications are in reasonable agreement with those determined for individual sources from VLBI measurements. Further it predicts a core-dominated fraction of sources as a function of flux density in excellent agreement with observation.

Four further remarks are important with respect to the current model:

(i) Although we chose LDDE to describe the evolution, it can be shown that due to the shape of the RLF *some* models of LDDE are exactly equivalent to PLE. Obviously a simple solution of PLE would be very interesting with regard to physical models for *all* AGN evolution (radio-loud and radio-quiet).

(ii) The model fit of LDDE has the lower-radio power FRIIs undergoing little or no evolution. By virtue of the correlation between line-strength and radio luminosity, these are inevitably of weak emission-line type. This suggests that the weak-lined FRIIs underwent a similar evolution history as FRIs; it is only the powerful strong-emission line FRIIs which evolved strongly with cosmic epoch. It might then be possible to define the two populations in terms of optical emission-line strength rather than radio morphology, the two emission-types perhaps representing different accretion types. Such a view has important ramifications for the process of physical evolution; and it may be that development of such a variant of the model could result in a single source function describing the entirety of the radio-source population.

(iii) Although the simple beaming models adopted provide a good description of the count data, there are other combinations of the Doppler beaming parameters which work. For example a very wide distribution of Lorentz factors also fits the GHz-frequency source counts and this variant was adopted by Urry and Padovani (1995). Ultimately our selection of parameters was made on the basis that the intrinsic core-to-extended flux ratio is an observed quantity and that the model distribution of  $R_{obs}$  values produced has the observed shape. In addition, the single  $\gamma$  value fitted in our model can be interpreted as modelling the mean value for the fastest material in the jets. The critical angles inferred from the successful models are  $\sim 8^\circ$  and  $\sim 5^\circ$  for the FRI and FRII populations respectively.

(iv) It must be borne in mind that the current model has been developed fundamentally with only three data sets: a source count at 151 MHz, a source count at 5 GHz, and a complete set of identifications and redshifts at 178 MHz. It is clear that the model can be improved. For example it predicts a low flux-density end of the 1.4-GHz count which is too high, and it predicts perhaps too few broad-line objects at low flux densities. Both deficiencies could be rectified with a local radio luminosity function for which the FRI component rolls off at somewhat lower powers than the current one, compensated by extending the FRII component to these lower powers.

However in view of the limited data from which the scheme was developed, its general success in describing much of the remaining data provides indication that the concept is substantially correct.

## REFERENCES

- Antonucci R., Miller J., 1985, ApJ, 297, 621
- Auriemma C., Perola G. C., Ekers R., Fanti R., Lari C., Jaffe W. J., Ulrich M.-H., 1977, AA, 57, 41
- Barthel P. D., 1989, ApJ, 336, 606
- Barthel P. D., 1994, in Bicknell G. V., Dopita M. A., Quinn P. J., eds, The First Stromlo Symposium: The Physics of Active Galaxies. ASP Conf Ser 54, p. 175
- Becker R. H., White R. L., Helfand D. J., 1995, ApJ, 450, 559
- Blandford R., Rees M., 1974, MNRAS, 169, 395
- Boyle B. J., Terlevich R. J., 1998, MNRAS, 293, L49
- Boyle B. J., Shanks T., Peterson B. A., 1988, MNRAS, 235, 935
- Browne I. W. A., Orr M. J. L., Davis R. J., Foley A., 1982, MNRAS, 198, 673
- Browne I. W. A., 1983, MNRAS, 204, L23
- Cohen M. H., Cannon W., Purcell G. H., Shaffer D. B., Broderick J. J., Kellermann K. I., Jauncey D. L., 1971, ApJ, 170, 207
- Condon J. J., 1984, ApJ, 287, 461
- Dallacasa D., Bondi M., Della Ceca R., Stanghellini C., 1997, Mem Soc astr Ital, 68, 55
- Davis R. J., Unwin S. C., Muxlow T. W. B., 1991, Nature, 321, 374
- Davis M. M., 1971, AJ, 76, 980
- de Ruiter H. R., Parma P., Fanti C., 1990, AA, 227, 351
- Donnelly R. H., Partridge R. B., Windhorst R. A., 1987, ApJ, 321, 94
- Doroshkevich A. G., Longair M. S., Zeldovich Y. B., 1970, MNRAS, 147, 139
- Dunlop J. S., Peacock J. A., 1990, MNRAS, 247, 19
- Fanaroff B. L., Riley J. M., 1974, MNRAS, 167, 31P

Fanti C., Fanti R., 1990, in Fanti C., Fanti R., O'Dea C. P., Schilizzi R. T., eds, CSS and GPS Radio Sources. CNR - Istituto di Radioastronomia Bologna, p. 215

Fanti C., Vigotti M., Di Paolo C., 1996, in Snellen I. A. G., Schilizzi R. T., Röttgering H., Bremer M. N., eds, The Second Workshop on GPS and CSS Radio Sources. Leiden Observatory, p. 38

Fomalont E. B., Windhorst R. A., Kristian J. A., Kellermann K. I., 1991, AJ, 102, 1258

Ghisellini G., Padovani P., Celotti A., Maraschi L., 1993, ApJ, 407, 65

Giovanini G., Feretti L., Venturi T., Kom K.-T., Kronberg P. P., 1993, ApJ, 406, 399

Giovanini G., Cotton W. D., Feretti L., Lara L., Venturi T., Marcaide J. M., 1995, in Cohen M. H., Kellermann K. I., eds, Quasars and AGN: High Resolution Imaging. Publ Nat Acad Sci, p. 11356

Gregory P. C., Condon J. J., 1991, ApJ supp, 75, 1011

Gruppioni G., Zamorani G., de Ruiter H. R., Palma P., Mignoli M., Lari C., 1997, MNRAS, 286, 470

Hales S. E. G., Baldwin J. E., Warner P. J., 1988, MNRAS, 234, 919

Hine R. G., Longair M. S., 1979, MNRAS, 188, 111

Kapahi V. K., Athreya R. M., Subrahmanya C. R., McCarthy P. J., van Breugel W., Baker J. C., Hunstead R. W., 1996, in Ekers R., Fanti C., Padrielli L., eds, Proc IAU Symp 175, Extragalactic Radio Sources. Kluwer Academic Publishers, p. 393

Kühr H., Pauliny-Toth I. I. K., Nauber U., 1981, AA supp ser, 45, 367

Kollgaard R. I., Wardle J. F. C., Roberts D. H., Gabuzda D. C., 1992, AJ, 104, 1678

Laing R. A., Peacock J. A., 1980, MNRAS, 190, 903

Laing R. A., Riley J. M., Longair M. S., 1983, MNRAS, 204, 151

Laing R. A., Wall J. V., Jenkins C. R., Unger S. W., 1994, in Bicknell G. V., Dopita M. A., Quinn P. J., eds, The First Stromlo Symposium: The Physics of Active Galaxies. ASP Conf Ser 54, p. 201

Ledlow M. J., Owen F. N., 1996, in Ekers R., Fanti C., Padrielli L., eds, Extragalactic Radio Sources. Kluwer Academic Publishers, p. 238

Longair M. S., 1966, MNRAS, 133, 421

Masson C. R., Wall J. V., 1977, MNRAS, 180, 193

Metcalfe N., Shanks T., Fong R., Roche N., 1995, MNRAS, 273, 257

Moffat A. T., Gubbay J., Robertson D. S., Legg A. J., 1972, in Evans D. S., ed, Proc IAU Symp 44: External Galaxies and Quasi-Stellar Objects. Reidel: Dordrecht, p. 228

Morganti R., Killeen N. E. B., Tadhunter C. N., 1993, MNRAS, 263, 1023

Morganti R., Oosterloo T. A., Reynolds J. E., Tadhunter C. N., Migenes V., 1997, MNRAS, 284, 541

Morisawa K., Takahara F., 1987, MNRAS, 228, 745

Murphy D., Browne I. W. A., Perley R. A., 1993, MNRAS, 264, 298

Orr M. J. L., Browne I. W. A., 1982, MNRAS, 200, 1067

Owen F. N., Ledlow M. J., Keel W. C., 1996, AJ, 111, 53

Pauliny-Toth I. I. K., Witzel A., Preuss E., Kühr H., Kellermann K. I., Fomalont E. B., Davis M. M., 1978, AJ, 83, 451

Pauliny-Toth I. I. K., Steppe H., Witzel A., 1980, AJ, 85, 329

Peacock J. A., Gull S., 1981, MNRAS, 196, 611

Peacock J. A., 1987, in Kundt W., ed, Astrophysical Jets and their Engines. Reidel: Dordrecht, p. 185

Perez-Fournon I., Biermann P., 1984, AA, 130, L13

Press W. H., Teukolsky S. A., Vetterling W. T., Flannery B. P., 1992, Numerical Recipes in Fortran. Cambridge University Press

Readhead A. C. S., 1995, in Cohen M. H., Kellermann K. I., eds, Quasars and AGN: High Resolution Imaging. Publ Nat Acad Sci, p. 11447

Rixon G. T., Wall J. V., Benn C. R., 1991, MNRAS, 251, 243

Robertson J. G., 1980, MNRAS, 190, 143

Roche N., Shanks T., Metcalfe N., Fong R., 1996, MNRAS, 280, 397

Rowan-Robinson M., Benn C. R., Lawrence A., McMahon R. G., Broadhurst T. J., 1993, MNRAS, 263, 123

Sadler E., Jenkins C. R., Kotanyi C. G., 1989, MNRAS, 240, 591

Saunders W., Rowan-Robinson M., Lawrence A., Efstathiou G., Kaiser N., Ellis R. S., Frenk C. S., 1990, MNRAS, 242, 318

Scheuer P. A. G., Readhead A. C. S., 1979, Nature, 277, 182

Scheuer P. A. G., 1987, in Zensus J. A., Pearson T. J., eds, Superluminal Radio Sources. Cambridge University Press, p. 104

Schmidt M., 1976, ApJ, 209, L55

Shaver P. A., Wall J. V., Kellermann K. I., Jackson C. A., Hawkins M. R. S., 1996, Nature, 384, 439

Shaver P. A., Hook I., Jackson C. A., Wall J. V., Kellermann K. I., 1998, in Carilli C., Radford S., Menten K., eds, Highly Redshifted Radio Lines. ASP Conf Ser, in press

Singal A. K., 1996, MNRAS, 278, 1069

Snellen I. A. G., 1997, PhD thesis, University of Leiden

Taylor G. B., Vermeulen R. C., Pearson T. J., 1995, in Cohen M. H., Kellermann K. I., eds, Quasars and AGN: High Resolution Imaging. Publ Nat Acad Sci, p. 11381

Urry C. M., Padovani P., 1995, PASP, 107, 803

Vermeulen R. C., 1995, in Cohen M. H., Kellermann K. I., eds, Quasars and AGN: High Resolution Imaging. Publ Nat Acad Sci, p. 0

Wall J. V., Jackson C. A., 1997, MNRAS, 290, 17P

Wall J. V., Peacock J. A., 1985, MNRAS, 216, 273

Wall J. V., Pearson T. J., Longair M. S., 1980, MNRAS, 193, 683

Wall J. V., 1980, Phil Trans R Soc, A296, 367

Wall J. V., 1994, Aust J Phys, 47, 625

Wall J. V., 1998, in Jackson N., Bremer M. N., Perez-Fournon I., eds, Observational Cosmology with the New Radio Surveys. Kluwer Academic Publishers, p. 129

Windhorst R. A., Miley G. K., Owen F. N., Kron R. G., Koo D. C., 1985, ApJ, 289, 494

Wrobel J. M., Krause S. W., 1990, ApJ, 363, 11

This paper has been produced using the Royal Astronomical Society/Blackwell Science L<sup>A</sup>T<sub>E</sub>X style file.